Journal of Alloys and Compounds 477 (2009) 547–551

Contents lists available at ScienceDirect

Journal of Alloys and Compounds

journal homepage: www.elsevier.com/locate/jallcom

Electrodeposition of RE–TM (RE = La, Sm, Gd; TM = Fe, Co, Ni) films and magnetic properties in urea melt

Jiaxin Li[a,b], Heng Lai[a], Biqiang Fan[a], Bin Zhuang[a], Lunhui Guan[b], Zhigao Huang[a,b,*]

[a] Department of Physics, Fujian Normal University, Fuzhou 350007, China
[b] Fujian Institute of Research on the Structure of Matter, Chinese Academy of Sciences, Fuzhou 350002, China

ARTICLE INFO

Article history:
Received 22 July 2008
Received in revised form 16 October 2008
Accepted 19 October 2008
Available online 12 December 2008

Keywords:
RE–TM films
Inductive codeposition
Magnetic properties
Microstructure

ABSTRACT

Rare earth (RE)—3d transition metal (TM) films were codeposited in low temperature urea–acetamide–NaBr–KBr–$RECl_3$–$TMCl_2$ baths by potentiostatic electrolysis. Cyclic voltammetry is used to investigate the electrochemical behavior of RE(III) and TM(II) in baths on a Pt electrode. The reduction of TM(II) is an irreversible process. RE(III) cannot be reduced alone, but it can be inductively codeposited with TM(II). Some kinetic parameters are measured, e.g., the transfer coefficient α and the diffusion coefficient D_0 for TM(II). It is reasonably suggested that the RE-induced codeposition ability and efficiency is dominated by the electronegativity difference between RE and TM atoms. Moreover, it is found that the surface morphologies, the magnetic anisotropy and preferring orientation of the as-deposited RE–TM films depend strongly on the composition and potential. At last, it is observed that, there exists a clear anisotropy with easy magnetization along the plane of the RE–TM films. The magnetic anisotropy in amorphous RE–TM films should be due to the competing contributions from several factors, such as spin–orbit coupling, stress, *etc.*

1. Introduction

A considerable number of studies have been made on RE–TM films due to their wide range of applications in magnetic, magneto-optical, and thermoelectric devices. For example, Sm–Fe alloy is found to exhibit giant magnetostriction for powerful transducer. Furthermore, it is used to fabricate the permanent magnet materials $Sm_2Fe_{17}N_x$ [1–4]; Gd–Co alloy is known to exhibit perpendicular magnetic anisotropy for magneto-optical recording media [5–8]; La–Ni alloy is usually used to form hydrogen storing functional material [9–11], *etc.* Up to now, RE–TM films are usually produced by the method of sputtering or melt casting, and the production processes are complex and costly [12–14]. Electrodeposition is an alternative method for preparing these films. It has the advantage of being simple, utilizing easily maintained equipment. The structure and magnetic properties of the deposited films can be controlled by changing solution composition and deposition conditions.

Recently, literature reports have focused on the electrodeposition of RE–TM from high-temperature molten salt [12–17], organic solutions [18–20] and aqueous solutions [21–23]. It is found that the first and second techniques are restricted from application because of its complex equipment, environmental pollution and the higher cost. Furthermore, high-temperature molten salt has not proven suitable for the formation of amorphous RE–TM alloys [15]. For the last one, all RE elements are very active since their reduction potentials range from −2.52 V to −2.25 V vs. SCE, which makes it very difficult to be deposited on electrodes. And hydrogen evolution is inevitable in the electrodeposition process, which lets the pH value shift to positive value and gives rise to the forming of the metal oxides [22]. Based on the above-mentioned reasons, a proper nonaqueous medium for metal electrodeposition, namely, a low-temperature urea molten salt has been selected [24–28]. The molten salt has lower eutectic point, higher conductivity, wider electrochemical window and greater solubility of metal chloride. Moreover, the urea molten salt system can remove impurity water and dissolve some metal oxides on the electrode surface.

In this work, we have studied the amorphous RE–TM films prepared by electrodeposition in a low-temperature urea molten salt. The experimental results reveal that the deposition mechanism of the RE and TM are coupled and complex. In addition, the effect of potential on the composition, microstructure and magnetic properties of RE–TM alloys is remarkable. Moreover, the magnetization mechanism on RE–TM films is discussed.

---

[*] Corresponding author at: Department of Physics, Fujian Normal University, Fuzhou 350007, China. Tel.: +86 591 23501062; fax: +86 591 22867395.
E-mail address: zghuang@fjnu.edu.cn (Z. Huang).

0925-8388/$ – see front matter © 2008 Elsevier B.V. All rights reserved.
doi:10.1016/j.jallcom.2008.10.157

2. Experimental details

All chemical reagents used are analytically pure in this experiment. Anhydrous $RECl_3$ (RE = La, Sm, Gd) was prepared by the reaction of RE_2O_3 (99.99%) and HCl aqueous solution (36.5%), and then the products were evaporated and dehydrated under vacuum at 393 K for 10 h. $TMCl_2$ (TM = Fe, Co, Ni) was obtained by the dehydration of $TMCl_2{\cdot}xH_2O$ under vacuum at 393 K for 10 h. Before use, urea and acetamide were dried under vacuum at 338 K for 5 h, NaBr and KBr were also dried under vacuum at 343 K for 5 h, respectively.

The voltammetry experiments were measured by electrochemical workstation. Argon was flushed through the bath, and the argon flow was maintained over the solution during the measurements. The working electrode was platinum (99.99%, 0.196 mm^2). A platinum foil was used as a counter-electrode. The reference electrode was an Ag/AgCl. All potential values determined in this paper were referenced to this electrode.

The electrodeposited experiments were carried out in a simple three-electrode glass cell with $RECl_3$ (0.100 mol L^{-1})–$TMCl_2$ (0.040 mol L^{-1})–urea (34.0 wt.%)–acetamide (50.0)–NaBr (14.0)–KBr (2.0). The temperature was controlled at 353 K by oil bath thermostat. The deposited time *t* with 25 min was chosen. The RE–TM films were deposited on Cu substrates (2.25 cm^2) by potentiostatic electrolysis under an Ar atmosphere, using graphite electrode (about 2.25 cm^2) as a counter-electrode. The compositions of the RE–TM films were determined by both inductive coupled plasma emission spectrometer (ICP) in JY-Ultima-2 and energy diffraction spectroscopy (EDS) in OXFORD6587. The crystal structures were analyzed by X-ray diffraction (XRD) in RIGAKU D/MAX2500. The surface morphologies were observed with scanning electron microscope (SEM) in JSM-6700F. The magnetic properties of the prepared films were measured by vibrating sample magnetometer (VSM).

3. Results and discussion

3.1. Electrochemical behavior for electrolyte

The electrochemical window of the background melt, based on a previous study [24,25], is 1.90 V. The reaction at the anodic limit appears to form polymeric products. However, at the cathodic limit it may do by the following Eq. (1) [28]:

$$R{-}CO{-}NH_2 + e \rightarrow 1/2H_2 + R{-}CO{-}NH^- \quad (R = NH_2,\ CH_3) \qquad (1)$$

Fig. 1 shows the cyclic voltammograms (CVs) of Pt electrode at different scan rates (υ) in the urea–acetamide–NaBr–KBr–$CoCl_2$ (0.040 mol L^{-1}) melt at 353 K. The cathodic peak potentials shift to a negative direction with increasing scan rate. The inset of Fig. 1 shows the cathodic peak potential (E_P) as a function of ln υ. From the figure, a good linearity is found, which indicates that the charge-transfer process is irreversible. For an irreversible charge-transfer electrode process: $|E_{P/2} - E_P| = 1.857RT/(\alpha nF)$, where $R, T, E_P, E_{P/2}, \alpha, n$ and F stand for gas constant, melt temperature, peak potential, half peak potential, transfer coefficient, electron transfer number and Faraday coefficient, respectively. From the figure, the values of E_P and $E_{P/2}$ can be obtained. So, together with $n = 2$, we can get $\alpha = 0.31$. The relationship between the peak current (i_p) and potential sweep rate (υ) can be described by $i_p = 0.4958nF(\alpha nFD_0\upsilon/RT)^{1/2}Ac$, where i_p, A, D_0 and c mean peak current, electrode area and diffusion coefficient, respectively. According to the former i_p formula and $i_p \sim \upsilon^{1/2}$ curve, we can get $D_0 = 4.78 \times 10^{-5}\ cm^2\ s^{-1}$.

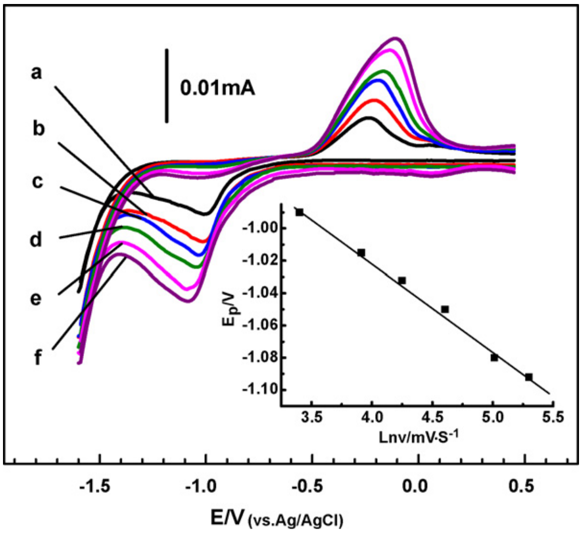

Fig. 1. CVs of Co(II) in acetamide–urea–NaBr–KBr melt at Pt electrode for $T = 353$ K with scan rate υ ($V s^{-1}$): (a) 0.03; (b) 0.05; (c) 0.07; (d) 0.10; (e) 0.15; (f) 0.20. The inset shows the deposition peak potential (E_P) as a function of ln υ.

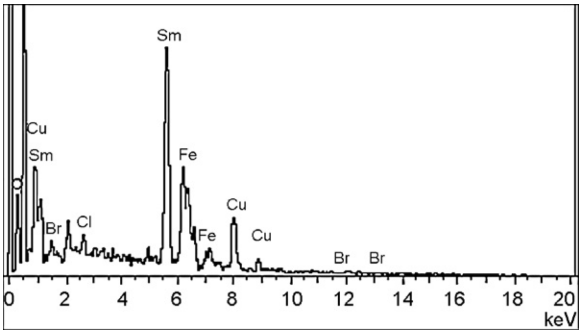

Fig. 2. EDS spectrum of as-deposited Sm–Fe film obtained by potentiostatic electrolysis.

Based on the above discussion, we can also get $\alpha = 0.39$ and 0.23, $D_0 = 7.58 \times 10^{-5}\ cm^2\ s^{-1}$, and $9.25 \times 10^{-6}\ cm^2\ s^{-1}$ for TM = Fe and Ni, respectively. Thus, the change of the values of α and D_0 can be found as follows: Fe(II) > Co(II) > Ni(II), being consistent with the value of the TM(II) electronegativity, which may predominate electrodeposition efficiency.

3.2. The induced codeposition of RE–TM films

Due to the shield effect of the inner electrons on the outer electrons, the attraction force of the nucleus to the outer electrons weakens. Therefore, all RE elements are very active since their reduction potentials are very negative, and this makes it very difficult to be deposited on electrodes from their urea melt baths. Furthermore, the standard electrode reduction potentials of Sm, Gd and La are −2.414 V, −2.397 V and −2.552 V vs. SCE, respectively, and the electrochemical window of the background melt is 1.90 V. In our previous study [24–26], we found that RE(III) (RE = Sm, La, Gd) cannot be reduced alone into metallic RE in urea melt, but can be inductively codeposited with TM(II). Hereinto, the deposited RE–TM films have been also analyzed by EDS and ICP, respectively. The measured results prove the discussion above.

Fig. 2 presents the EDS spectrum of as-deposited Sm–Fe film and the composition is shown in Table 1. Here, Cu and C elements from the substrate and carbon double-sided conductive tape have been eliminated in computation, respectively. The deposit consists of Sm, Fe, and a small amount of other elements, such as Cl and Br, which come from the residual salts adhered to the surface. From the EDS, a pure Sm–Fe film deposited from urea melt is prepared. The urea melt can remove impure water by itself owing to the hydrolyzation of urea at $T > 334$ K (that is, $CO(NH_2)_2 + H_2O = CO_2\uparrow + 2NH_3\uparrow$), as well

Table 1
The composition of the Sm–Fe deposit (eliminating Cu element).

	Elements			
	Fe	Sm	Cl	Br
wt.%	13.83	81.52	1.51	3.14
at.%	28.46	62.21	4.82	4.51

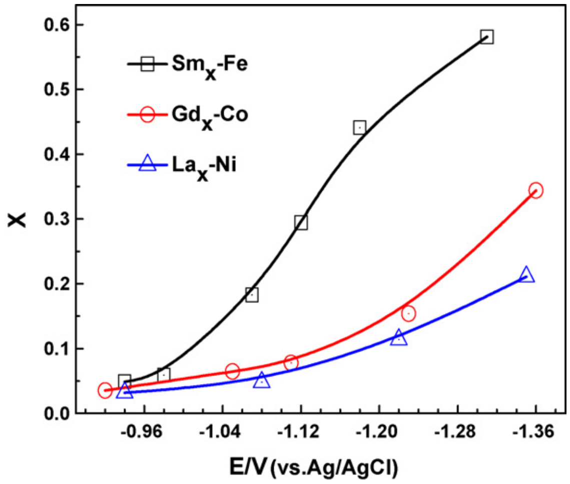

Fig. 3. The dependence of RE content of RE–TM deposits on electrodepositon potential.

as dissolve some metal oxides on the electrode surface [28], so the oxidation will not occur during the electrolysis. Of course, there may be a small amount of oxidation in the RE–TM films. However, O spectrum from RE–TM film surface is not clearly observed due to small content.

Fig. 3 shows the RE content analyzed by ICP as a function of electrodepositon potential for the deposited RE–TM films. From the figure, it is found that the RE contents of the RE–TM films increases with decreasing applied potential (to shift negatively). At the same time, it is found that, when the potential is far away from −1.38 V, the electrode reaction becomes fast and the induced reduction of RE(III) becomes complicated, which results in the quick increase of TM(II) and the sharp decrease of RE content [28]. So, the deposition potential would be selected between −0.90 V and −1.40 V in our experiment.

Although the induced codeposition mechanism is not very clear now, extensive research has been carried out substantially. For example, Liu et al. [28] suggested the induced codeposition of Sm–Co alloys in urea melt may relate to the formation of the polynuclear complex of Sm(III) and Co(II) which are presented in the electrolyte as electroactive intermediates. It is considered that there exists a functional group, –NCO–, in the melt system, and RE and TM have a strong affinity with oxygen and nitrogen, respectively. Thus, a heteronuclear complex may be formed, and it acts as a electroactive species in the electrolyte.

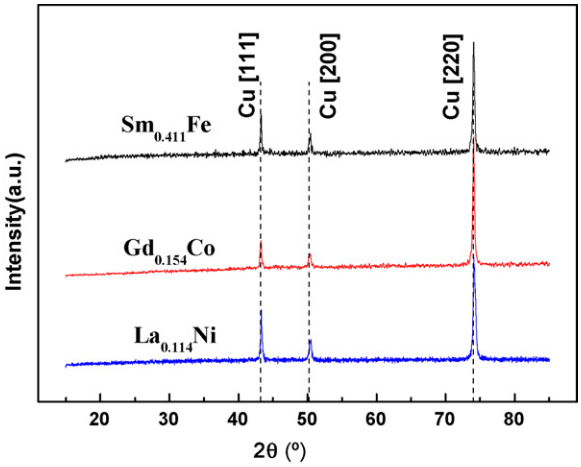

Fig. 4. XRD patterns of as-deposited RE–TM films.

We think that the above-mentioned vierpoints are reasonable. However, we also find that the RE contents in the deposited RE–TM alloys are associated with the electronegativity difference between RE and TM atoms [29]. When the applied potential is maintained in the range with −0.94 V to −1.36 V, the RE deposited content increases with decreasing applied potential (to shift negatively). Moreover, one notices that, for the same potential, Sm content with Fe (Sm_xFe) > Gd content with Co (Gd_xCo) > La content with Ni (La_xNi), as shown in Fig. 3. In our previous studies on Sm–Co and Sm–Fe alloys [24,25], the similar rule has been found. That is, in the same potential, Sm content for Sm_xFe is more than that for Sm_xCo. Compared to these results, the induced codeposition mechanism can be explained as follows: the ability that the atoms attract electrons is controlled by the electronegativity. TM atom absorbs some electrons from RE atoms in electrolyte, which results in the reduction potentials of RE to shift positively. So, the RE and TM potentials

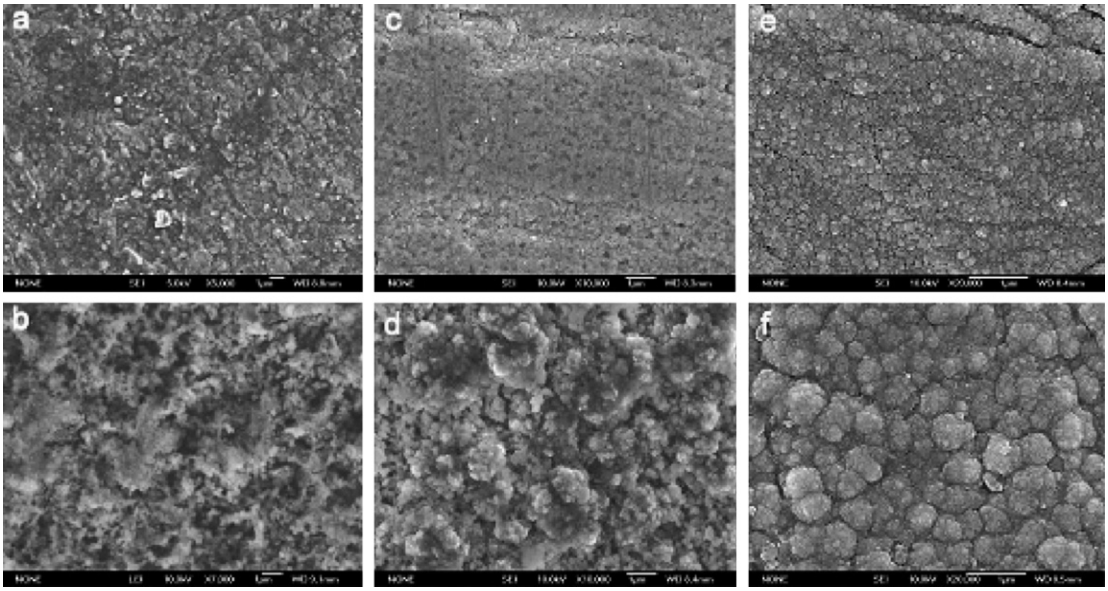

Fig. 5. SEM patterns of as-deposited RE_xTM films: (a) $Sm_{0.049}Fe$; (b) $Sm_{0.411}Fe$; (c) $Gd_{0.035}Co$; (d) $Gd_{0.154}Co$; (e) $La_{0.032}Ni$; (f) $La_{0.114}Ni$.

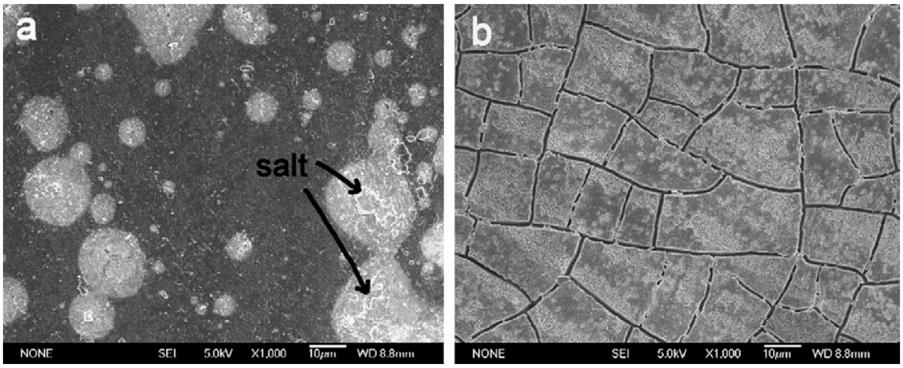

Fig. 6. SEM patterns of as-deposited Sm_xFe films at low magnification: (a) $Sm_{0.049}Fe$ and (b) $Sm_{0.411}Fe$.

become closer, and the induced codeposition of the RE element can be implemented. Thus, we can reasonably conclude that the RE-induced codeposition ability and efficiency are dominated by the electronegativity difference between RE and TM atoms.

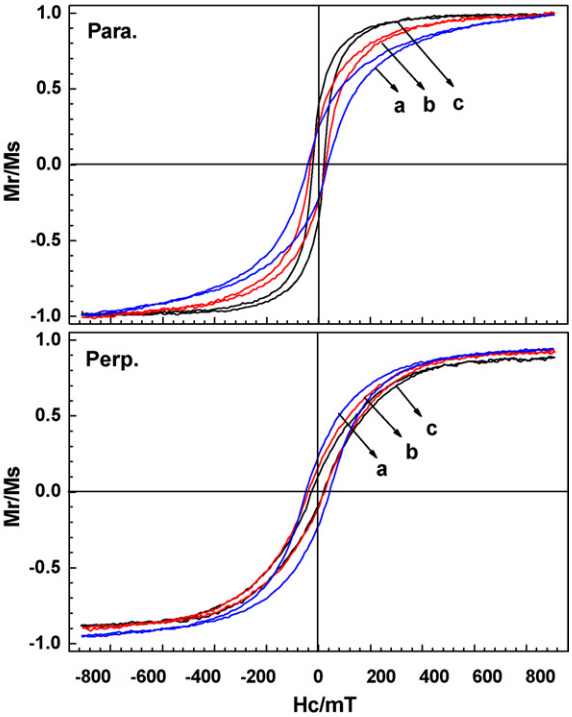

Fig. 7. Hysteresis loops of as-deposited Sm_xFe films under the applied magnetic field parallel (||) and perpendicular (⊥) to the film at room temperature: (a) $x = 0.411$; (b) $x = 0.183$; (c) $x = 0.049$.

3.3. XRD and SEM of RE–TM films

Fig. 4 shows XRD patterns of the as-deposited RE–TM ($Sm_{0.411}Fe$, $Gd_{0.154}Co$ and $La_{0.114}Ni$) films. For all of the three patterns, it is found that the diffraction peaks from Cu (1 1 1), (2 0 0) and (2 2 0) were identified and no other peaks were detected. The results are consistent with uncovered Cu substrate, which indicates that the as-deposited RE–TM films are all amorphous. Those are consistent with the other experimental results [7,21,28].

Fig. 5(a)–(f) shows the SEM patterns of as-deposited $Sm_{0.049}Fe$, $Sm_{0.411}Fe$, $Gd_{0.035}Co$, $Gd_{0.154}Co$, $La_{0.032}Ni$ and $La_{0.114}Ni$, respectively. Fig. 6(a) and (b) shows the SEM patterns of as-deposited $Sm_{0.049}Fe$ and $Sm_{0.411}Fe$ with low magnification, respectively. Comparing the patterns of the samples with low RE content to those with higher RE content, e.g., Fig. 5(a) with (b), (c) with (d), (e) with (f), we find that, the samples with low RE content are smooth, compact and homogeneous without any cracks; while those with higher RE content have larger surface roughness and less adhesion strength. For the samples with higher RE content, some fine cracks do even appears, as seen in Fig. 6(b). However, there exist also the uniform and rounded nanoparticles in $La_{0.032}Ni$ alloy, as shown in Fig. 5(e), and the bigger spheric grains in $La_{0.114}Ni$ alloy, as seen in Fig. 5(f), which may be due to the lower deposition efficiency and the lower La content. Moreover, it is observed that there is no any apparent cracks found in La–Ni alloys. Thus, the SEM results reveal that the deposition surface morphology is related to the deposited composition.

3.4. Magnetic properties of amorphous RE–TM films

Fig. 7 shows the typical hysteresis loops of as-deposited Sm_xFe ($x = 0.411$, 0.183, 0.049) films under the magnetic field parallel (||) and perpendicular (⊥) to the plane at room temperature. Gd–Co and La–Ni alloys have similar hysteresis loops. From the loops, it is found that all RE–TM films show smooth hysteresis loops. The coercivity (H_c) and remanence ratio S (Mr/Ms) of the RE_xTM films with different RE composition for both || and ⊥ cases are listed

Table 2

H_c and S (Mr/Ms) for RE–TM alloy films with different compositions and deposition potentials for ⊥ and || direction to the film plane at room temperature.

Sample	Smx–Fe			Gdx–Co			Lax–Ni		
E/V	−0.94	−1.11	−1.18	−0.92	−1.23	−1.36	−0.94	−1.08	−1.22
x	0.049	0.183	0.411	0.035	0.154	0.344	0.032	0.048	0.114
H_c ($\times 10^{-3}$ T)									
⊥	22.1	31.7	45.8	26.3	25.6	28.3	20.5	20.9	21.5
||	21.6	29.2	38.5	21.8	21.9	22.4	19.2	20.1	21.0
S (Mr/Ms)									
⊥	0.111	0.146	0.249	0.107	0.119	0.127	0.221	0.212	0.369
||	0.374	0.267	0.249	0.436	0.419	0.347	0.736	0.707	0.551

in Table 2. From Fig. 7 and Table 2, it is found that the values of $H_c^{\perp}$ are greater than H_c, and the values of $S^{\perp}$ are less than that of $S^{||}$, which means that there exists a clear anisotropy, and easy magnetization direction is along in the plane of the film. Furthermore, it is observed that the values of $H_c^{\perp}$ and H_c for Sm–Fe alloys increase evidently with increasing Sm content. However, the values of $H_c^{\perp}$ and H_c for Gd–Co and La–Ni alloys change gently. Also, the remanence ratio S displays a strong RE content dependence. With increasing RE content, the values of $S^{\perp}$ increase evidently and those of $S^{||}$ decrease obviously, which means that the magnetic anisotropy decreases obviously. The magnetic anisotropy in RE–TM amorphous films should be due to the competing contributions from several factors, such as spin–orbit coupling, stress, *etc.* [30].

4. Conclusions

The amorphous RE–TM films on Cu substrates in urea melt at 353 K through potentiostatic electrolysis have been synthesized. The contents, microstructures and magnetic properties with different potential have been measured. The induced codeposition mechanism, and the magnetization behavior have been investigated. The results are summarized as follows:

1. It have been obtained that, for TM = Fe, Co, Ni, $\alpha = 0.39$, 0.31, 0.23 and $D_0 = 7.58 \times 10^{-5}\,\text{cm}^2\,\text{s}^{-1}$, $4.78 \times 10^{-5}\,\text{cm}^2\,\text{s}^{-1}$, $9.25 \times 10^{-6}\,\text{cm}^2\,\text{s}^{-1}$, respectively. So, the values of α and D_0 varied as follows: Fe(II) > Co(II) > Ni(II).
2. The reduction of TM(II) is an irreversible process. RE(III) cannot be reduced alone, but it can be inductively codeposited with TM(II). The codeposition process may involve a polynuclear complex containing TM(II) and RE(III), presenting in the electrolyte as electroactive intermediates. Moreover, in the same potential, Sm content for Sm_xFe > Gd content for Gd_xCo > La content for La_xNi. At last, we can reasonably conclude that the RE induced codeposition ability and efficiency are dominated by the electronegativity difference between RE and TM atoms.
3. From the SEM patterns, we find that, the samples with low RE content are smooth, compact and homogeneous without any cracks; while those with higher RE content have larger surface roughness and less adhesion strength.
4. It is also found that, for the as-deposited RE–TM films prepared by urea melt, the values of $H_c^{\perp}$ are greater than those of H_c, and the values of $S^{\perp}$ are less than those of $S^{||}$, which means that there exists a clear anisotropy, and easy magnetization direction is along the plane of the film. The magnetic anisotropy in RE–TM amorphous films should be due to the competing contributions from several factors, such as spin–orbit coupling, stress, *etc.*

Acknowledgements

The authors would like to thank Prof. Z. Chen (Experiment Center, Fujian Normal University) and Dr. X.P. Wu (Department of Chemistry, Fuzhou University) for experiments. This work was supported by NSF of China under Grant No. 60676055, NSF of Fujian Province (A0510013) and National Key Project for Basic Research of China (No. 2005CB623605).

References

[1] J.M.D. Coey, H. Sun, J. Magn. Magn. Mater. L251 (1990) 87.
[2] E. Sarantopoulou, S. Kobe, K.Z. Rozman, Z. Kollia, G. Drazic, A.C. Cefalas, IEEE Trans. Magn. 2943 (2004) 40.
[3] K.Z. Rozman, P.J. McGuiness, B. Podmiljsak, M. Rajic, S. Kobe, IEEE Trans. Magn. 2952 (2004) 40.
[4] Y.X. Tong, P. Liu, L.Z. Liu, Q.Q. Yang, J. Rare Earths 275 (2001) 19.
[5] O.S. Anilturk, A.R. Koymen, J. Magn. Magn. Mater. 272 (2004) 531.
[6] L. Martinot, D. Leroy, H. Zhan, C. Licour, C. Jerome, G. Chapelle, C. Calberg, R.J. Jeromeb, Mater. Chem. 729 (2000) 10.
[7] G.R. Li, C.W. Xu, Y.X. Tong, G.K. Liu, J. Rare Metals 304 (2004) 28 (2).
[8] G.P. Zheng, Y.W. Zhan, P. Liu, J. Alloys Compd. 65 (2003) 358.
[9] M.Z. An, J.L. Wang, D.Z. Sun, J. Appl. Electrochem. 891 (2001) 31.
[10] S.K. Pandey, A. lSrivastava, O.N. Srivastava, J. Hydrogen Energy 2461 (2007) 32.
[11] A. Rudajevova, D. Vasylyev, O. Musi, Physica B 758 (2006) 378.
[12] C. Prados, A. Hernando, G.C. Hadjipanayis, J.M. Gonzalez, J. Appl. Phys. 6148 (1999) 85.
[13] R. Andreescu, M.J. O'Shea, J. Appl. Phys. 8183 (2002) 91.
[14] J. Sayama, K. Mizutani, T. Asahi, J. Ariake, K. Ouchi, S. Mastunuma, T. Osaka, J. Magn. Magn. Mater. 239 (2005) 287.
[15] T. Iida, T. Nohira, Y. Ito, Electrochim. Acta 2537 (2001) 46.
[16] T. Iida, T. Nohira, Y. Ito, Electrochim. Acta 901 (2003) 48.
[17] T. Iida, T. Nohira, Y. Ito, J. Alloys Compd. 207 (2005) 386.
[18] D.S. Yuan, G.K. Liu, Y.X. Tong, J. Electroanal. Chem. 123 (2002) 536.
[19] G.R. Li, Y.X. Tong, G.K. Liu, J. Electroanal. Chem. 223 (2004) 562.
[20] G.R. Li, Q.F. Ke, G.K. Liu, Y.X. Tong, Mater. Lett. 60 (2006) 2611.
[21] M. Schwartz, N.V. Myung, K. Nobe, J. Electrochem. Soc. C468 (2004) 151.
[22] J.Q. Zhang, P. Evans, G. Zangari, J. Magn. Magn. Mater. 89 (2004) 283.
[23] W. Zhu, S.L. Wang, Rare Met. Mater. Eng. 37 (2008) 891.
[24] J.X. Li, H. Lai, Z.C. Zhang, B. Zhuang, Z.G. Huang, Acta Phys.-Chim. Sin. 1301 (23) (2007) 8.
[25] J.X. Li, Z.G. Huang, Z.C. Zhang, B. Zhuang, H. Lai, Rare Met. Mater. Eng., in press.
[26] H. Lai, J.X. Li, W.C. Zhou, B. Zhuang, X.P. Wu, Z.G. Huang, Rare Met., in press.
[27] S.L. Wang, J.B. Lin, Q.Y. Cai, Y. Zhang, J. Alloys Compd. 450 (2008) 142.
[28] P. Liu, Y.P. Du, Q.Q. Yang, Y.X. Tong, G.A. Hope, J. Electrochem. Soc. c57 (2006) 153.
[29] L. Pauling, in: J.X. Lu, Y.Z. Huang (Eds.), The Nature of the Chemical Bond and Structure of Molecules and Crystals: An Introduction to Modern Structure Chemistry, Shanghai, Shanghai Scientific & Technical Publishers, 1981, Interpret.
[30] R.C. O'handley, Modern Magnetic Materials Principles and Applications, John Wiley & Sons, 2000;
Y.Q. Zhou, et al., interpret, Chemical Industry Press (CIP), 2002.